Research article

The nano-artificial periosteum made of PCL/MgO/AS-IV enhances MC3T3-E1 cell osteogenic differentiation and promotes bone defect repair via the EphB4/EphrinB2 signaling pathway

Wei Wang [a], Dan-Fang Sun [b], Hui-Xia Cui [c], Wen-Lu Zhang [c, *]

[a] *North Jiangsu Health Management Center of Zhongshan Hospital Affiliated to Fudan University, Yancheng, 224100, China*
[b] *Jinzhou Medical University, Jinzhou, 121000, China*
[c] *The First Affiliated Hospital of Wannan Medical College (Yijishan Hospital), 241004, Wuhu, China*

A B S T R A C T

Bone regeneration plays a pivotal role in periodontal tissue repair. With advancements in biotechnology materials, the utilization of nanotechnology offers a reliable platform for bone restoration in periodontitis. In this study, we successfully established a long-term bacterial infection model using *Porphyromonas gingivalis* (*P. gingivalis*) with MOI = 50. CCK-8 and ROS immunofluorescence results demonstrated that the combined effect of Mg^{2+} and AS-IV significantly enhanced cell proliferation and effectively suppressed the inflammatory response during bacterial infection. Alkaline phosphatase and alizarin red staining revealed that the synergistic action of Mg^{2+} and AS-IV notably promoted osteogenic differentiation of MC3T3-E1 cells under *P. gingivalis*-infected conditions. Considering the properties of these two biomaterials, we fabricated polycaprolactone (PCL) artificial periosteum loaded with MgO and AS-IV using an electrostatic spinning technique. The findings indicated that PCL/MgO/AS-IV artificial periosteum exhibited excellent biocompatibility and hydrophilicity, thereby substantially enhancing cellular adhesion to its surface as well as augmenting cellular value-added rate. Moreover, efficient drug release from the PCL/MgO/AS-IV artificial bone membrane conferred remarkable antimicrobial activity along with in vitro osteogenic potentiality. The in vivo experiments conducted on animals further substantiated the exceptional properties exhibited by PCL/MgO/AS-IV artificial periosteum in bone defect repair. Additionally, it was observed that PCL/MgO/AS-IV artificial periosteum could modulate EphB4-EphrinB2 signaling to enhance osteogenic differentiation under *P. gingivalis*-infected conditions.This exciting outcome suggests that PCL/MgO/AS-IV artificial periosteum holds great promise as a biomaterial for treating periodontal bone loss.

1. Introduction

The pathogenesis of periodontitis, an infectious periodontal disease caused by plaque biofilm infection, is significantly influenced by the involvement of *P.gingivalis* [1]. The clinical manifestation of periodontitis in patients is typically characterized by progressive degradation of periodontal soft and hard tissues, ultimately leading to tooth loss [2]. As one of the most prevalent human diseases, severe periodontitis affects up to 11 % of individuals worldwide [3,4]. The application of Guided Tissue Regeneration (GTR) and

Guided Bone Regeneration (GBR) has become commonplace in the treatment of periodontal disease, wherein a barrier membrane is utilized to facilitate the regeneration of periodontal tissues. Notably, Bio-Gide stands as an exemplary representative in this technique [5]. However, this collagen membrane is primarily sourced from mammalian collagen, which not only poses risks associated with infectious disease transmission but also exhibits limitations concerning immune response and religious considerations [6]. Furthermore, considering that bacterial infection is the primary causative agent of periodontitis and inadequate control of pathogenic bacteria is the main factor contributing to failure in GTR/GBR procedures, the utilization of a barrier membrane becomes indispensable. Hence, it is crucial to emphasize the antimicrobial properties of the barrier membrane. Although antibiotics are effective in combating bacterial infections, their excessive use not only leads to resistance but also results in various side effects [7]. Therefore, it is clinically significant to screen antimicrobial agents and develop composites with excellent biocompatibility, antimicrobial activity, and osteogenic effects for treating periodontitis. In recent years, electrostatic spunlace membranes have gained significant traction in the biomedical field owing to their exceptional attributes such as a substantial specific surface area, remarkable porosity, and excellent chemical stability [8]. Polycaprolactone (PCL) is an FDA-approved biomaterial that possesses exceptional biocompatibility, biodegradability, anti-inflammatory properties, and osteogenic potential. It finds extensive applications in drug delivery systems, fracture fixation, and cellular engineering [9]. Moreover, PCL is extensively utilized in drug delivery systems, fracture immobilization, and cell engineering due to its remarkable shape memory temperature control characteristics. Consequently, it is considered a promising precursor for polymer composite material applications [10,11]. The antimicrobial and bone-enhancing properties of magnesium oxide (MgO) make it a promising dental antimicrobial agent with potential for clinical application [12]. Additionally, MgO can be efficiently metabolized and absorbed in the body, minimizing adverse effects. Upon degradation, it releases biologically active magnesium ions (Mg^{2+}) that facilitate osteoblast adhesion, enhance alkaline phosphatase (ALP) activity, and promote the expression of osteogenic differentiation-related proteins crucial for bone remodeling [13]. Studies have demonstrated that MgO-doped PCL materials exhibit potent antimicrobial activity against *Escherichia coli* (*E. coli*) and *Staphylococcus aureus* (*S. aureus*), while also stimulating the proliferation of human periodontal ligament stem cells and augmenting osteogenic differentiation processes [14,15]. Furthermore, MgO stands out among other metal oxides for biomedical applications owing to its dual antimicrobial and osteogenic properties [16].

Astragaloside IV (AS-IV), the primary bioactive compound derived from the Chinese herb Astragalus, exhibits fibrinolytic properties and inhibits endotoxin development. Additionally, AS-IV enhances immune response, possesses anti-inflammatory and antioxidant effects [17,18]. In LPS-induced periodontitis, AS-IV prevents apoptosis of human periodontal ligament cells and exerts a protective influence on periodontal tissues [19]. Bone remodeling is a dynamic process involving osteoblasts and osteoclasts, regulated by multiple signaling pathways [20]. The EphrinB2-EphB4 bidirectional signaling pathway plays a crucial role in bone remodeling, angiogenesis promotion, and neurological disorders. Its forward signaling inhibits osteoclast differentiation while reverse signaling promotes osteoblast differentiation, which has garnered significant attention from scholars [21,22]. AS-IV has been found to inhibit RANKL-mediated osteoclastogenesis and enhance the osteogenic differentiation of MC3T3-E1 cells through the PI3K-AKT signaling pathway [23,24]. Furthermore, an experiment on rat tibial defects confirmed that AS-IV enhances the osteogenic function of bone marrow mesenchymal stem cells through the miR-124-3p.1/STAT3 axis and promotes the repair of rat tibial defects [25]. MgO has been reported to synergize with various drugs in promoting osteoblast cell differentiation [26,27]. Therefore, we postulated that the combination of AS-IV and MgO could potentially exert a synergistic effect on promoting osteogenic differentiation while also exhibiting antimicrobial activity. However, there is limited research on MgO-loaded and AS-IV artificial periosteum currently available. More experimental evidence is needed to explore the role of PCL/MgO/AS-IV in bone defect repair.

2. Materials and methods

2.1. Cell culture and treatment

The MC3T3-E1 mouse precursor osteoblasts (Shanghai, China) were cultured in α-MEM supplemented with 10 % FBS (Gibco, Australia) and 1 % penicillin (Hyclone, China) at 37 °C. For the induction of osteogenic differentiation, cells were cultured for a duration of up to 21 days using an osteogenic induction medium composed of 10 mmol/L sodium β-glycerophosphate, 0.1 μmol/L dexamethasone, and 50 mg/L ascorbic acid.

2.2. Bacteria and culture conditions

The *P.gingivalis* stock (ATCC33277; Laboratory of Oral Biology, China Medical University) was thawed and inoculated onto a BHI solid anaerobic blood agar plate with a bacterial ring. It was then cultured anaerobically at 37 °C for 6–7 days. A single colony exhibiting robust growth was selected for liquid enrichment, followed by low-speed centrifugation (3000 rpm/min). The pellet obtained after centrifugation was washed 2–3 times with PBS and re-suspended in 15 ml centrifuge tubes. The resulting colony forming units (CFU)/ml were determined at an optical density of 600 nm using an ultraviolet spectrophotometer (Beckman Coulter), and the bacterial numbers were calculated from the OD values using the formula: bacterial density = OD value × dilution × 10^9. Subsequently, the bacterial solution was resuspended within double-antibody-free α-MEM medium and the bacterial MOI was adjusted for subsequent experiments.

2.3. Bacterial MOI selection

The MC3T3-E1 cell suspension was inoculated at a density of 3×10^3 cells per well in 96-well plates, followed by the inoculation of *P.*

gingivalis with varying multiplicities of infection (MOIs) including 0, 50, 100, 200, and 500 into the stabilized attached cells in the same plates. For bacterial inoculation, cells were washed with PBS and then co-cultured with *P.gingivalis* in a constant temperature incubator at 37 °C for 1 h. Subsequently, the cells were treated with 100 μg/ml metronidazole and 300 μg/ml gentamicin (Procell, China) to eliminate extraneous bacteria before being incubated in fresh medium. The control group underwent the same culture medium change and conditions without the addition of *P.gingivalis*. Cell viability was determined using CCK-8 kit after 24 h. Absorbance at 450 nm was measured using a multifunctional enzyme marker (Thermo, USA) and the results were recorded.

2.4. Bacterial inoculation

MC3T3-E1 cells grown to logarithmic growth phase were taken and stabilized by 24 h of adherence to the wall. *P.gingivalis* with a multiplicity of infection (MOI) of 50 was then inoculated into well plates at two-day intervals, while employing the antibiotic protection method for cell washing during each inoculation. The cells were cultured for durations of 7, 14, and 21 days.

2.5. CCK-8 detects cytotoxicity

The cells were pre-cultured in 96-well plates with an inoculation of 3×10^3 cells per well, and after 24 h of cell attachment stabilization, they were infected with *P.gingivalis*. The experiment consisted of two groups: the blank control group (MC3T3-E1) and the *P. gingivalis* infection group (MC3T3-E1+*P.gingivalis*). The *P.gingivalis*-infected cells were cultured for 7, 14, and 21 days respectively, and the original culture was discarded. Cytotoxicity was assessed by measuring absorbance at 450 nm using a multifunctional enzyme marker, and the results were recorded.

2.6. Live and dead cell staining to detect cell activity

The cells were inoculated in 6-well plates at a density of 1×10^5 cells per well, and the experimental groups were established following previously described protocols. After 24 h of cell attachment stabilization, the cells were infected with *P.gingivalis*. Subsequently, the infected cells were cultured for 7, 14, and 21 days respectively, while discarding the original culture medium. The staining effect of the cells was evaluated using the Calcein/PI Assay Kit (Beyotime, China) according to the manufacturer's instructions, and observed under a fluorescence microscope.

2.7. CCK-8 assay for proliferative activity of MC3T3-E1 cells

The experiment was divided into five groups: ① blank group (MC3T3-E1), ② *P.gingivalis* infection group (MC3T3-E1+*P.gingivalis*), ③ *P.gingivalis* + Mg^{2+} group (MC3T3-E1+*P.gingivalis* + Mg^{2+}), ④ *P.gingivalis* + AS-IV group (MC3T3-E1+*P.gingivalis* + AS-IV), and ⑤ *P.gingivalis* + Mg^{2+}+AS-IV group (MC3T3-E1+*P.gingivalis* + Mg^{2+} + AS-IV). Cells were pre-cultured in a 96-well plate by inoculating at a density of 3×10^3 cells per well, and after allowing the cells to adhere for 24 h, they were incubated with 2 mM Mg^{2+} and 40 μg/ml AS-IV for different time points of 24, 48, and 72 h respectively; four sub-wells were set up in each experimental group. Cell viability was assessed using a CCK-8 kit according to the manufacturer's instructions, and absorbance at 450 nm was measured using a multifunctional enzyme marker.

2.8. Morphological changes in cells

The cells were inoculated at a density of 1×10^5 per well in 6-well plates, and the experimental groups were established following previously described protocols. After the cell apposition was stabilized, the cells in each group were infected with Porphyromonas gingivalis except the blank group, while based on the grouping, the cells in each group were cultured with culture medium containing Mg^{2+} and AS-IV respectively. Subsequently, the changes in cell morphology were observed after 72 h under a light microscope.

2.9. Immunofluorescence detection of ROS expression in MC3T3-E1 cells

The MC3T3-E1 cells were seeded in 6-well plates at a density of 1×10^5 cells per well. After infection with *P.gingivalis* for 7 days, the culture was discarded. Subsequently, each well was treated with 2 ml of DCFH-DA (Solaibio, China) and incubated in a controlled environment for 15 min. Following three washes with serum-free culture medium, the samples were examined under a fluorescence microscope to assess ROS expression.

2.10. Alkaline phosphatase staining to observe ALP activity

The MC3T3-E1 cells were seeded at a density of 1×10^5 cells per well in 6-well plates. After 14 days of culture, the original medium was discarded and the cells were fixed with 4 % paraformaldehyde for 20 min at room temperature. Subsequently, the cells were washed three times with PBS. ALP staining was performed using an alkaline phosphatase staining kit (Beyotime, China) according to the manufacturer's instructions, followed by microscopic observation to assess ALP activity expression.

2.11. Alizarin red staining for mineral content

The MC3T3-E1 cells were seeded at a density of 1×10^5 cells per well in 6-well plates. After 21 days of culture, the original medium was discarded and the cells were fixed with 4 % paraformaldehyde for 30 min at room temperature. Subsequently, the wells were washed three times with PBS and incubated with 2 ml of alizarin red stain (Beyotime, China) for 30 min at room temperature. Following this, the wells were washed three times with PBS and examined under a microscope to assess mineral deposition.

2.12. Electrostatic spinning to make artificial periosteum

The AS-IV (90 mg) was completely dissolved in 1 mL of DMSO and set aside. Subsequently, the MgO (18 mg) was dispersed in 9 mL of hexafluoroisopropanol solution (HFIP), followed by sonication for 2 h to achieve uniform dispersion. Then, dropwise addition of the aforementioned mixture of DMSO and AS-IV was performed into the prepared mixture of HFIP and MgO with thorough stirring. Finally, 1.8 g of PCL was added and stirred overnight at room temperature to obtain a homogeneous electrostatic spinning solution. Pure PCL, PCL-MgO, and PCL-AS-IV electrospinning solutions were prepared using the same ratio as above and set aside. The prepared electrospinning solution was loaded into a 5 mL syringe attached to a propulsion pump, while applying a voltage of 10 kV to the needle with a propulsion speed set at 1 m/h, collection speed at 10 rpm, and collection distance at 20 cm. The resulting composites were vacuum-dried for two days to ensure complete removal of organic solvent.

2.13. Characterization of artificial periosteum

The morphology of the material after gold spraying on the surface of the fabricated ICMs was observed through scanning electron microscopy (SEM) tests. X-ray diffraction (XRD, D/max 2550V, Rigaku, Japan) was employed to characterize the crystal structure of the ICMs. FTIR analysis was conducted to identify the functional groups present in the ICMs. Furthermore, hydrophilicity investigation of the ICMs involved utilizing static droplet technique and calculating their water contact angle (WCA). Photographic documentation corresponding to these experiments was captured using a light microscope (CX40PSUNNY).

2.14. Soaking experiment

In order to investigate the degradation of the artificial periosteum and the release of active ingredients in vitro, each set of samples (2.5×5 cm) was weighed and recorded as initial weight (W0). Subsequently, all samples were fully immersed in a container containing 10 mL of phosphate-buffered saline (PBS) and sealed on a constant temperature shaker at 37 °C. The medium was completely replaced every week, and at predetermined time points, the samples were removed, washed with deionized water, dried, and their weights were measured and recorded as Wt. The degradation rate (%) was calculated using the equation: Degradation rate (%) = (W0 - Wt)/W0 × 100.

2.15. Drug and ion release

To assess the release of active ingredients from the artificial periosteum, uniform-sized pieces weighing 10 mg were prepared and fully immersed in a 10 mL container filled with PBS. The container was then placed on a constant temperature shaker at 37 °C. At predetermined time intervals, 1 mL of the medium was withdrawn and replaced with an equal volume of fresh PBS. The concentration of AS-IV in the liquid was determined using a UV spectrophotometer at 450 nm to calculate cumulative release. Additionally, analysis by inductively coupled plasma atomic emission spectrometry (ICPAES) was employed to determine the release of Mg^{2+} from the artificial periosteum in PBS medium at different time points.

2.16. Effect of PCL/MgO/AS-IV on cell proliferation viability

The artificial periosteum was initially shaped into a 14 mm diameter circle prior to the commencement of the experiment. Subsequently, it underwent sterilization by immersion in a 75 % ethanol solution for 1 h and UV irradiation for 30 min. Cells were co-cultured with sterilized artificial periosteum in 24-well plates at a density of 1×10^4 cells per well, and the original culture medium was discarded after 48 h. The absorbance at 450 nm was measured using the CCK-8 kit following the manufacturer's instructions, and the results were recorded.

2.17. Cell morphology and adhesion

The experiment was divided into five groups: ① blank control group (PCL), ② P.gingivalis group (P.gingivalis + PCL), ③ PCL/MgO group (P.gingivalis + PCL/MgO), ④ PCL/AS-IV group (P.gingivalis + PCL/AS-IV), and ⑤ PCL/MgO/AS-IV group (P.gingivalis + PCL/MgO/AS-IV). Cells were inoculated at a density of 5×10^4/well in sterilized artificial periosteum-coated 24-well plates, and the original culture medium was replaced after incubation for 24 h. Subsequently, the cells were fixed with 4 % formaldehyde for half an hour, permeabilized with 0.1 % TritonX-100 for 15 min, stained with fluorescein using ghost pen cyclic peptide (Solaibio, China) for 20 min, counterstained with DAPI (Solaibio, China) for 10 min to visualize nuclei under a fluorescence microscope and record images accordingly; additionally, scanning electron microscopy was employed to observe cell morphology following dehydration by alcohol

gradient.

2.18. Antibacterial activity

The experimental groups were as follows: ① *P.gingivalis* group, (*P.gingivalis* + PCL) ② PCL/MgO group (*P.gingivalis* + PCL/MgO), ③ PCL/AS-IV group (*P.gingivalis* + PCL/AS-IV), and ④ PCL/MgO/AS-IV group (*P.gingivalis* + PCL/MgO/AS-IV). Each artificial perios-teum was individually immersed in a bacterial solution of *P. gingivalis* for 48 h. Subsequently, the bacterial suspensions from each group were separately spread on BHI agar plates and incubated at 37 °C under anaerobic conditions for 7 days to evaluate antibacterial activity based on colony counts.

2.19. Alkaline phosphatase staining to detect osteogenic activity

The experiment was divided into the following five groups: ① control group (PCL), ② *P.gingivalis* group (*P.gingivalis* + PCL), ③ PCL/MgO group (*P.gingivalis* + PCL/MgO), ④ PCL/AS-IV group (*P.gingivalis* + PCL/AS-IV), and ⑤ PCL/MgO/AS-IV group (*P.gingivalis* + PCL/MgO/AS-IV). After a culture period of 14 days, the original culture medium was discarded, and cells were fixed with 4 % paraformaldehyde for 20 min at room temperature followed by three washes with PBS. Subsequently, an alkaline phosphatase staining kit was used to stain the cells for a duration of 15 min according to the manufacturer's instructions. Finally, the stained samples were observed under a microscope and photographed.

2.20. Alizarin red staining for detection of osteogenic mineralization

The experimental grouping was conducted according to previously established protocols, and the cells were cultured for a duration of 21 days. Subsequently, the original culture medium was discarded and fixed using a 4 % paraformaldehyde solution for a period of 30 min. Following this fixation step, the wells were thoroughly washed three times with phosphate-buffered saline (PBS). Each well was then incubated with 2 ml of alizarin red staining solution at room temperature for 30 min. After another round of washing with PBS, microscopic observations were made by capturing photographs.

2.21. In vivo osteogenesis experiment

In order to investigate the osseointegration ability of artificial periosteum, in vivo osteogenesis experiments were conducted. Firstly, round-shaped PCL and PCL/MgO/AS-IV artificial periosteum with a diameter of 5 mm were fabricated, followed by ultraviolet light irradiation for 40 min and sterilization through soaking in 75 % ethanol for 2 h. Three 8-week-old healthy SD rats were selected and anesthetized with pentobarbital. The rats were positioned prone on the operating table, and the hair on the cranial vertex was removed. A 2 cm incision was made along the midline, followed by separation of the subcutaneous fascia. Subsequently, a round full-layered bone defect measuring 5 mm in diameter was created bilaterally and implanted into artificial periosteum. After an 8-week period, euthanasia was performed, and Micro-CT imaging was conducted. To evaluate biosafety, major organs from experimental animals were collected for histopathological examination using H&E staining to detect any potential pathological changes.

2.22. Detection of EphB4-EphrinB2 expression and osteogenic differentiation-related proteins via immunoprotein blotting

The experimental groups were classified as previously described, and the cells were cultured for 7 days. Subsequently, the medium was discarded and total protein was extracted using a RIPA lysing buffer (without inhibitors) and quantified with a BCA Kit (Beyotime, China), following the manufacturer's instructions. Aliquots of 28 μg protein were separated by PAGE (Beyotime, China), transferred to PVDF membranes (Millipore, USA), blocked with 5 % skimmed milk powder for 2 h, and incubated overnight at 4 °C with primary antibody. After washing four times with TBST, the membranes were incubated at room temperature for 2 h with HRP-conjugated goat anti-rabbit IgG (1:10,000). Finally, they were developed using an ECL substrate luminescence Kit (Beyotime, China). Primary anti-bodies were anti-β-Actin (CellSignaling Technology, USA), anti-EphB4 polyclonal antibody (CellSignaling Technology, USA), anti-EphrinB2 polyclonal (Abcam,USA), anti-ALP polyclonal (Abcam, USA), anti-OPN polyclonal (Proteintech, USA) and anti-Runx2 polyclonal (Proteintech, USA).

2.23. Statistical analysis

We used SPSS 25.0 software (IBM, Armonk, NY) for all analyses. Data are expressed as mean ± standard deviation. Two-way ANOVA and single-factor ANOVA were used to test group differences. Between-group comparisons were conducted by using the Neuman-Keuls (SNK) test and Student's t-test. We considered $p < 0.05$ to indicate statistical significance.

3. Results

3.1. Cell proliferation viability remains unaffected by P. gingivalis infection

As shown in Fig. 1A, the CCK-8 assay showed that *P.gingivalis* with MOI = 50 had no significant effect on cell growth compared with

the control group, but cell proliferation was significantly inhibited with the increase in MOI of *P.gingivalis*. Therefore, we chose *P. gingivalis* with MOI = 50 for subsequent experiments. As shown in Fig. 1B, CCK-8 assay results demonstrated that *P.gingivalis* infection after 7, 14, and 21 days induced some apoptosis but had no significant impact on cell proliferation when compared to the control group. In Fig. 1C and D, MC3T3-E1 cells were infected with *P.gingivalis* at an MOI of 50 for 7, 14, and 21 days. Live dead cell staining revealed a slight increase in the number of dead cells in the *P.gingivalis*-infected group compared to the control group on days 7, 14, and 21; however, these differences did not reach statistical significance.

3.2. AS-IV and Mg^{2+} promoted the proliferation of MC3T3-E1 cells under P.gingivalis infection

As depicted in Fig. 2A, the CCK-8 assay revealed a non-significant increase in cell count within the *P.gingivalis*-infected group after 24 h compared to the control group, while a decrease was observed at 48 and 72 h. However, when compared to the *P.gingivalis*-infected group, the combination of Mg^{2+} and AS-IV significantly enhanced time-dependent cell proliferation. Furthermore, as illustrated in Fig. 2B, cellular morphology analysis demonstrated crumpling and slight reduction in cell density within the *P.gingivalis* infected group relative to the control group; nevertheless, this effect was effectively reversed by co-treatment with Mg^{2+} and AS-IV resulting in restored cellular morphology characterized by pike and swirl arrangement along with a substantial increase in cell density.

3.3. AS-IV and Mg^{2+} reduce the inflammatory response of cells in the infected state of P.gingivalis

As depicted in Fig. 3A and B, the immunofluorescence assay revealed a significant upregulation of intracellular ROS expression in the *P.gingivalis*-infected group compared to the control group. However, treatment with Mg^{2+} and AS-IV resulted in a substantial reduction in intracellular ROS levels when compared to the *P.gingivalis*-infected group, indicating that the combined intervention
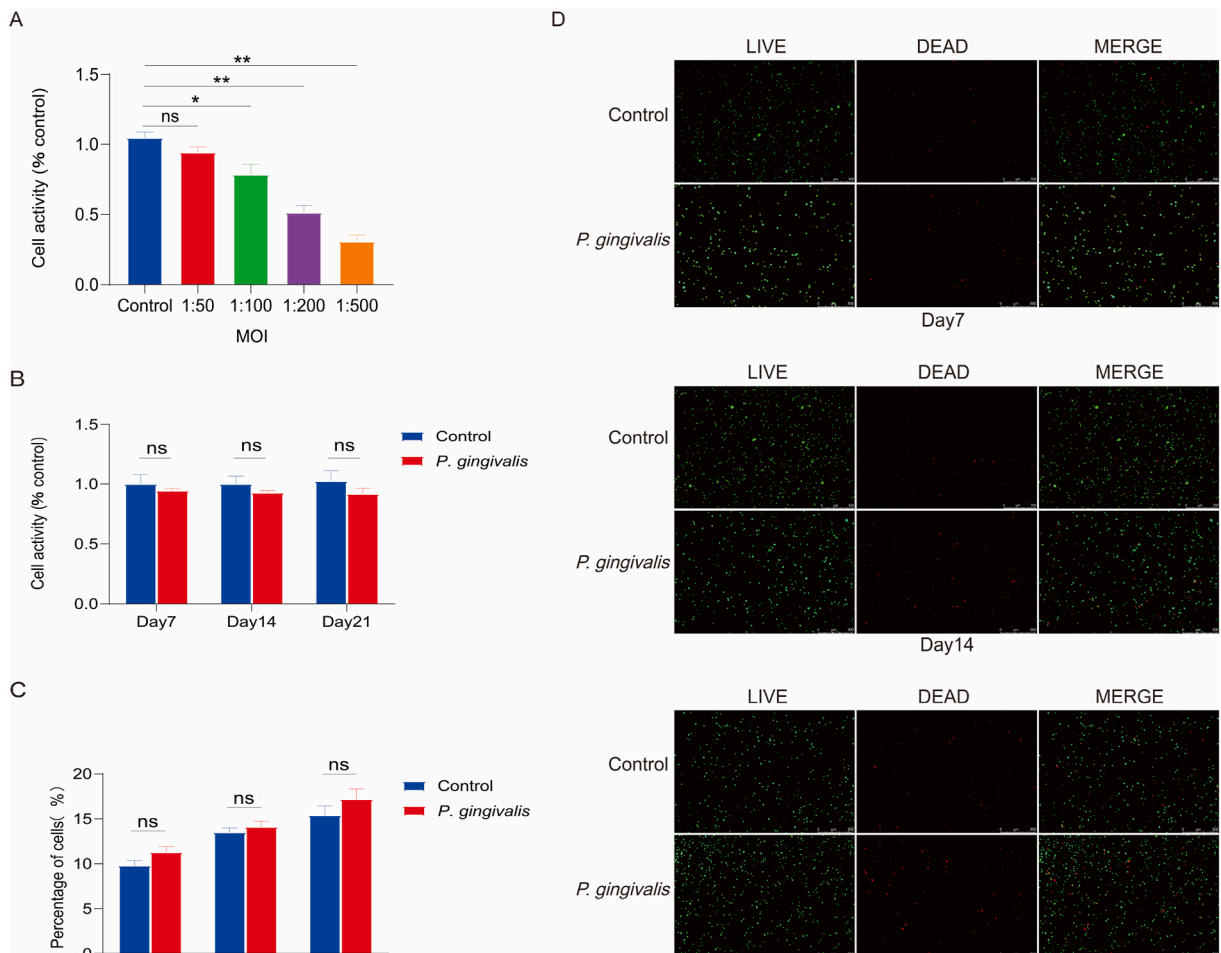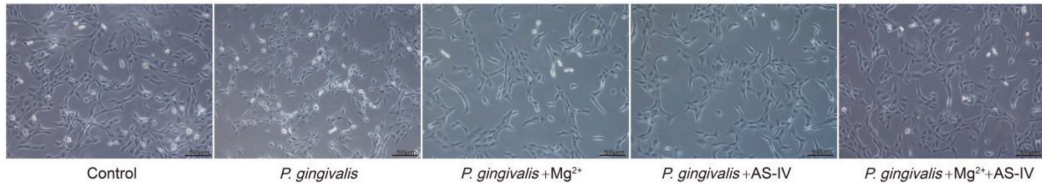

Fig. 1. Impact of P. gingivalis infection on the proliferation of MC3T3-E1 cells. (A) *P.gingivalis* with MOI = 50 had no significant effect on cellular value added. MC3T3-E1 cells were infected with *P. gingivalis* for 7, 14, and 21 days, respectively. (B) The CCK-8 assay demonstrated a non-significant decrease in cell numbers in the *P. gingivalis*-infected group compared to the control group. (C–D) Quantification of live-dead cell staining revealed no significant increase in apoptosis between the *P. gingivalis*-infected group and the control group. (*$p < 0.05$;**$p < 0.01$;ns $p > 0.05$).
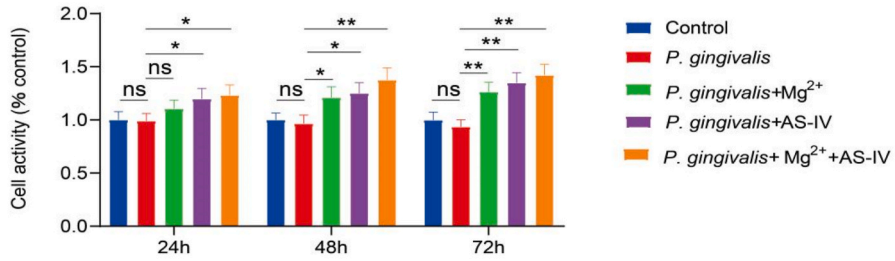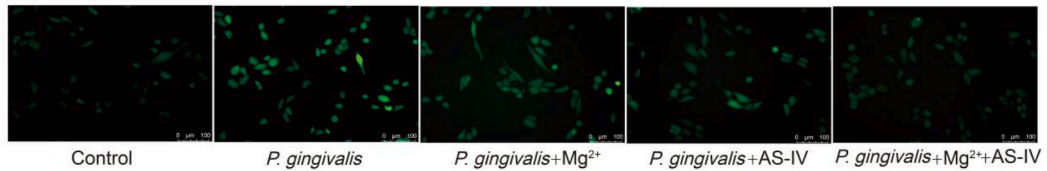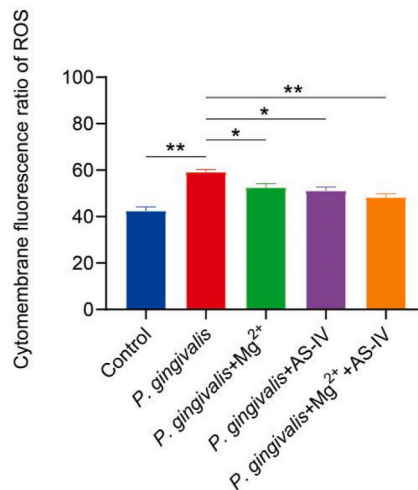
Fig. 2. Effects of AS-IV and Mg^{2+} on MC3T3-E1 cell proliferation in the presence of *P.gingivalis* infection. (A) CCK-8 assay demonstrated a significant synergistic effect of Mg^{2+} and AS-IV, promoting MC3T3-E1 cell proliferation during *P.gingivalis* infection. (B) Morphological analysis revealed that both Mg^{2+} and AS-IV effectively improved the growth status of MC3T3-E1 cells under *P.gingivalis* infection, leading to enhanced cell proliferation. (*$p < 0.05$;**$p<0.01$;ns $p>0.05$).

Fig. 3. Effects of AS-IV and Mg^{2+} on intracellular ROS expression in MC3T3-E1 cells under *P.gingivalis* infection status. (A) Immunofluorescence analysis and (B) quantitative results revealed a significant increase in intracellular ROS expression in the *P.gingivalis*-infected group, whereas the combined treatment with Mg^{2+} and AS-IV effectively suppressed intracellular ROS levels. (*$p < 0.05$;**$p<0.01$;ns $p>0.05$).

effectively mitigated *P.gingivalis*-induced mitochondrial damage and restored mitochondrial function within infected cells.

3.4. AS-IV and Mg^{2+} enhanced osteogenic differentiation of MC3T3-E1 cells

As shown in Fig. 4A and C, a cell culture period of up to 14 days was employed to assess the osteogenic differentiation activity of cells through alkaline phosphatase staining. The results revealed a significant reduction in osteogenic differentiation activity among *P. gingivalis*-infected cells compared to the control group; however, the presence of Mg^{2+} and AS-IV enhanced osteogenic differentiation under *P.gingivalis* infection conditions. Notably, the combined treatment with Mg^{2+} and AS-IV exhibited the most pronounced effect on promoting osteogenic differentiation and effectively counteracted the inhibitory impact of *P.gingivalis* infection on MC3T3-E1 cell's osteogenic potential.

### 3.5. AS-IV and Mg^{2+} enhanced the deposition of mineral content in osteoblasts

As depicted in Fig. 4B and D, cells were cultured for 21 days followed by alizarin red staining to assess intracellular mineral content. The findings revealed a significant reduction in bone deposition within the *P.gingivalis*-infected group compared to the control group. However, the presence of Mg^{2+} and AS-IV notably enhanced intracellular mineral deposition, with the combined effects of Mg^{2+} and AS-IV resulting in the most pronounced mineral deposition.
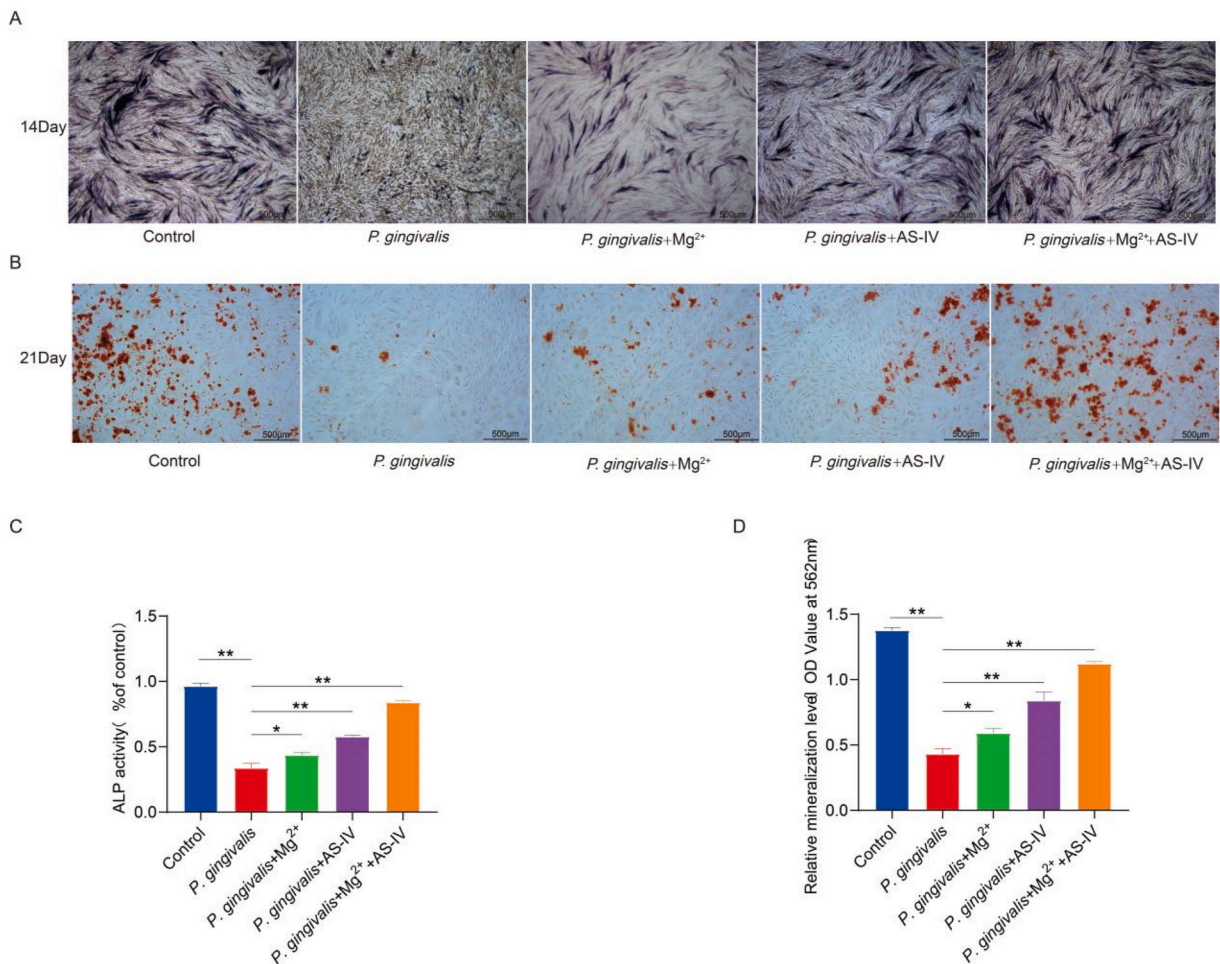
Fig. 4. Effects of Mg^{2+} and AS-IV on cellular ALP activity and osteogenic calcification during *P.gingivalis* infection. *P. gingivalis* infection of MC3T3-E1 cells for 14 days, (A) alkaline phosphatase staining and its quantification (C) results showing that the combined effect of Mg^{2+} and AS-IV can effectively increase the ALP activity of osteoblasts in the infected state of *P. gingivalis*. P. gingivalis infected MC3T3-E1 cells for 21 days, (B) alizarin red staining and its quantitative results (D) show that the combined effect of Mg^{2+} and AS-IV significantly promotes the deposition of mineral content in osteoblasts under *P. gingivalis* infection. (*$p < 0.05$;**$p < 0.01$;ns $p > 0.05$). (For interpretation of the references to colour in this figure legend, the reader is referred to the Web version of this article.)

3.6. Characterization of electrospun supports and water contact angle

The surface of the electrostatically spun artificial periosteum fibers was observed to be smooth and uniform, with no bead joints or adhesion between the fibers. Additionally, the overall distribution remained uniform and the fiber surface appeared smooth and flat (Fig. 5A). X-ray diffraction analysis of the artificial periosteum revealed a sharp diffraction peak at $2\theta = 42.821°$ for magnesium oxide particles, indicating their highly crystalline nature. Furthermore, two major diffraction peaks at $2\theta = 21.401°$ and $23.791°$ were observed for PCL in all groups of artificial periosteum samples (Fig. 5B). Notably, characteristic peaks corresponding to MgO were detected in both PCL/MgO group and PCL/MgO/AS-IV group, confirming successful addition of MgO particles. However, no changes in characteristic peaks were observed in the PCL/AS-IV group compared to the PCL group due to small content and uniform dispersion of AS-IV within the electrospinning solution. FTIR spectra analysis (Fig. 5C) confirmed presence of pcl in each artificial periosteum sample through observation of a characteristic peak located at 1720 cm^{-1} corresponding to C=O stretching vibration. Moreover, an absorption peak at 896 cm^{-1} representing C–H out-of-plane bending vibration of aromatic hydrocarbons was evident only in both PCL/ MgO/AS-IV group and PCL/AS-IV group, indicating successful addition of AS-IV into these two groups. The water contact angle results are presented in Fig. 5D, illustrating the water contact angles of the PCL group, PCL/MgO group, PCL/AS-IV group, and PCL/MgO/AS-
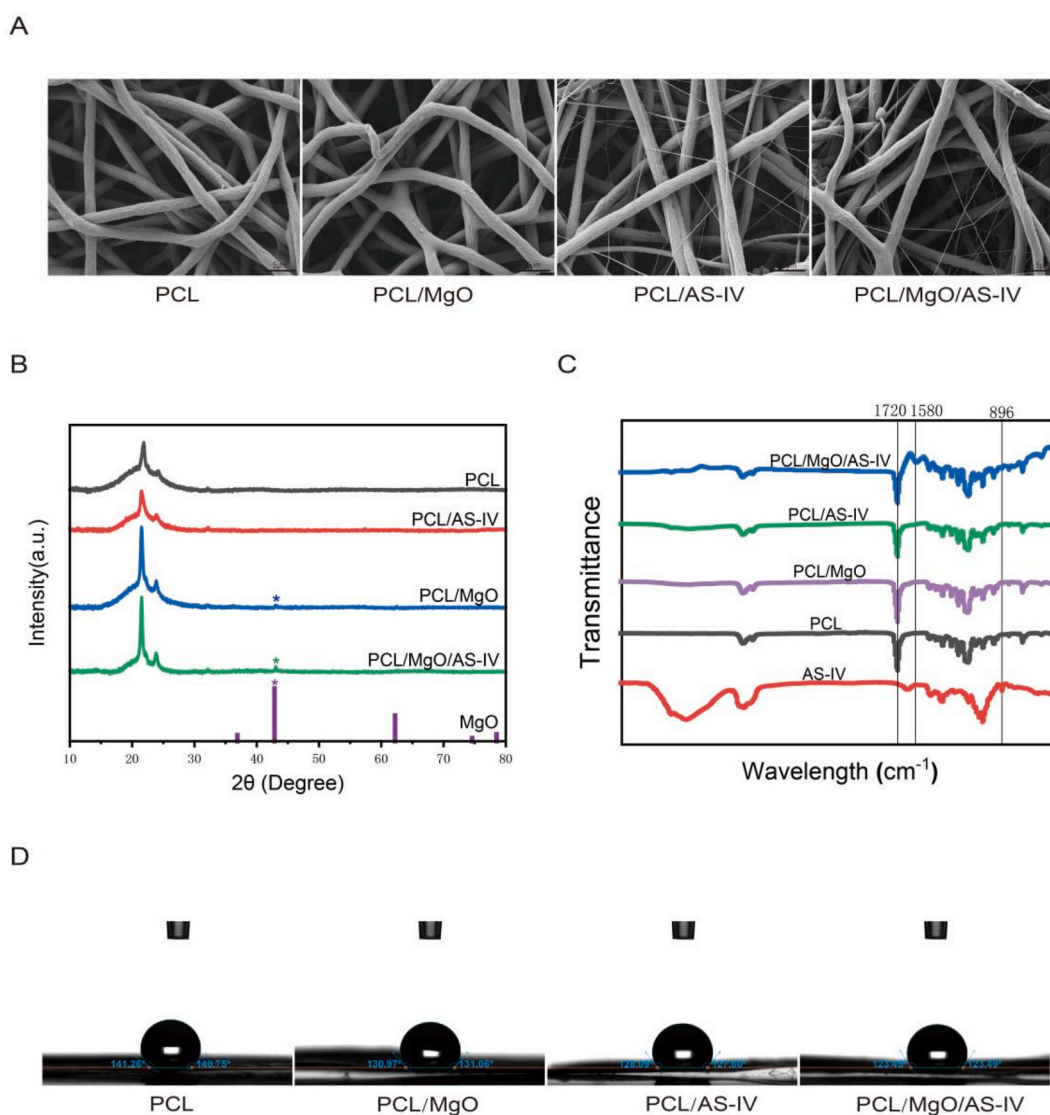
Fig. 5. Characterization of artificial periosteum using scanning electron microscopy and water contact angle analysis. (A) Scanning electron microscopy revealed that the morphology of materials in each group remained smooth, with no significant changes observed after the addition of MgO and AS-IV compared to the PCL group. (B) XRD analysis confirmed characteristic peaks corresponding to MgO in both the PCL/MgO group and PCL/ MgO/AS-IV group. (C) FTIR assay demonstrated successful incorporation of AS-IV into the artificial periosteum. (D) Water contact angle measurements indicated a decrease in water contact angle upon addition of MgO and AS-IV to the artificial periosteum.

IV group as 141°, 131°, 128°, and 123° respectively. It is evident that the incorporation of both MgO and AS-IV leads to a reduction in the hydrophobicity of PCL, thereby promoting favorable cell adhesion and growth.

3.7. Degradation of artificial periosteum and release of magnesium ions and AS-IV

The weight change of artificial periosteum degradation in vitro is illustrated in Fig. 6A, demonstrating that the incorporation of MgO or AS-IV into PCL accelerates the degradation rate of artificial periosteum. In vitro drug release profiles for the PCL/AS-IV and PCL/MgO/AS-IV groups are presented in Fig. 6B, revealing an initial burst release of AS-IV within the first 3 days, with over 50% released into the medium for both groups. Over time, AS-IV release reached 81.3 % and 89.7 % at 21 days in the PCL/AS-IV and PCL/MgO/AS-IV groups respectively. Fig. 6C depicts the release of Mg^{2+} during in vitro degradation of artificial periosteum. The release of Mg^{2+} during the in vitro degradation of artificial periosteum is illustrated in Fig. 6C. The entire process can be roughly categorized into three stages: an abrupt release in the initial stage, a rapid release in the intermediate stage, and a gradual release in the late stage. In the first 3 days, when the release rate was higher, Mg^{2+} release reached 49.3 % and 62.7 % for PCL/MgO and PCL/MgO/AS-IV groups respectively. By day 7, Mg^{2+} release reached 69 % and 76 % for these two groups respectively. Subsequently, there was a decline in the rate of Mg^{2+} release which eventually stabilized by day 14 until the end of the experiment on day 21.

3.8. PCL/MgO/AS-IV has good biocompatibility for MC3T3-E1 cells

As depicted in Fig. 7A, the CCK-8 assay revealed that cell proliferation was suppressed in the *P.gingivalis*-infected group compared to the PCL group. However, in the presence of bacterial infection, the PCL/MgO/AS-IV group significantly enhanced cell proliferation, demonstrating a statistically significant difference. Furthermore, as illustrated in immunofluorescence Fig. 7B and scanning electron microscopy results Fig. 7C, all groups exhibited well-adhered cells with excellent spreading on the membrane surface. The cells displayed expanded morphology with numerous pseudopods protruding from the material's surface.

### 3.9. PCL/MgO/AS-IV inhibited the activity of P.gingivalis

As depicted in Fig. 8A, the results of the in vitro antimicrobial assay demonstrated robust bacterial growth characterized by multiple black clusters in the *P.gingivalis* group. Furthermore, all experimental groups exhibited commendable antimicrobial efficacy compared to the *P.gingivalis* group; notably, the PCL/MgO/AS-IV group displayed superior performance by significantly inhibiting bacterial proliferation.

3.10. PCL/MgO/AS-IV promotes osteogenic differentiation under P.gingivalis infection

Fig. 9A, 9C and 9B, 9D demonstrate a significant reduction in ALP activity and mineral deposition in *P.gingivalis*-infected cells compared to the control group, as indicated by alkaline phosphatase and alizarin red staining. Furthermore, both the PCL/MgO group and the PCL/AS-IV group exhibited enhanced ALP activity and mineral content deposition compared to the *P.gingivalis*-infected group; however, it was observed that the PCL/MgO/AS-IV group exerted the most pronounced effect on osteogenic differentiation by effectively promoting ALP activity expression and bone matrix deposition under conditions of *P.gingivalis* infection.

3.11. Reconstruction of bone defects enhanced by PCL/MgO/AS-IV artificial periosteum

To further investigate the in vivo osteogenic capacity of PCL/MgO/AS-IV artificial periosteum, a cranial bone defect model was established, and PCL and PCL/MgO/AS-IV were implanted to fill the bone defects, respectively. As shown in Fig. 10A, The Micro-CT results at 8 weeks postoperatively revealed a significantly higher level of new bone production in the PCL/MgO/AS-IV periosteum compared to the PCL group, exhibiting superior coverage of the bone defect repair area. The Micro-CT analysis results in Fig. 10B demonstrate a significantly higher BV/TV ratio in the PCL/MgO/AS-IV periosteum group compared to the PCL group ($P < 0.05$), indicating enhanced osteogenesis. Consistent trends were also observed for bone trabeculae and BS/TV measurements, supporting the
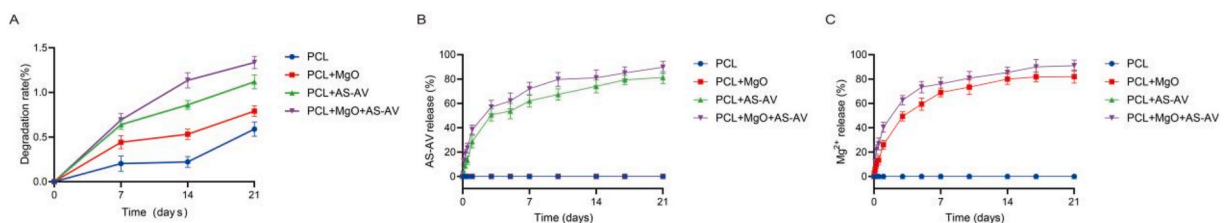

Fig. 6. Illustrates the degradation of the artificial periosteum and the release of magnesium ions and AS-IV from it. (A) Degradation experiments revealed that the inclusion of MgO and AS-IV accelerated the degradation rate of the artificial periosteum. (B) The drug release results demonstrated an initial burst release behavior for AS-IV, followed by a gradual decrease in release rate during later stages. (C) The Mg^{2+} release results exhibited an abrupt initial release behavior, which reached a relatively steady state after 14 days.

A

B

C
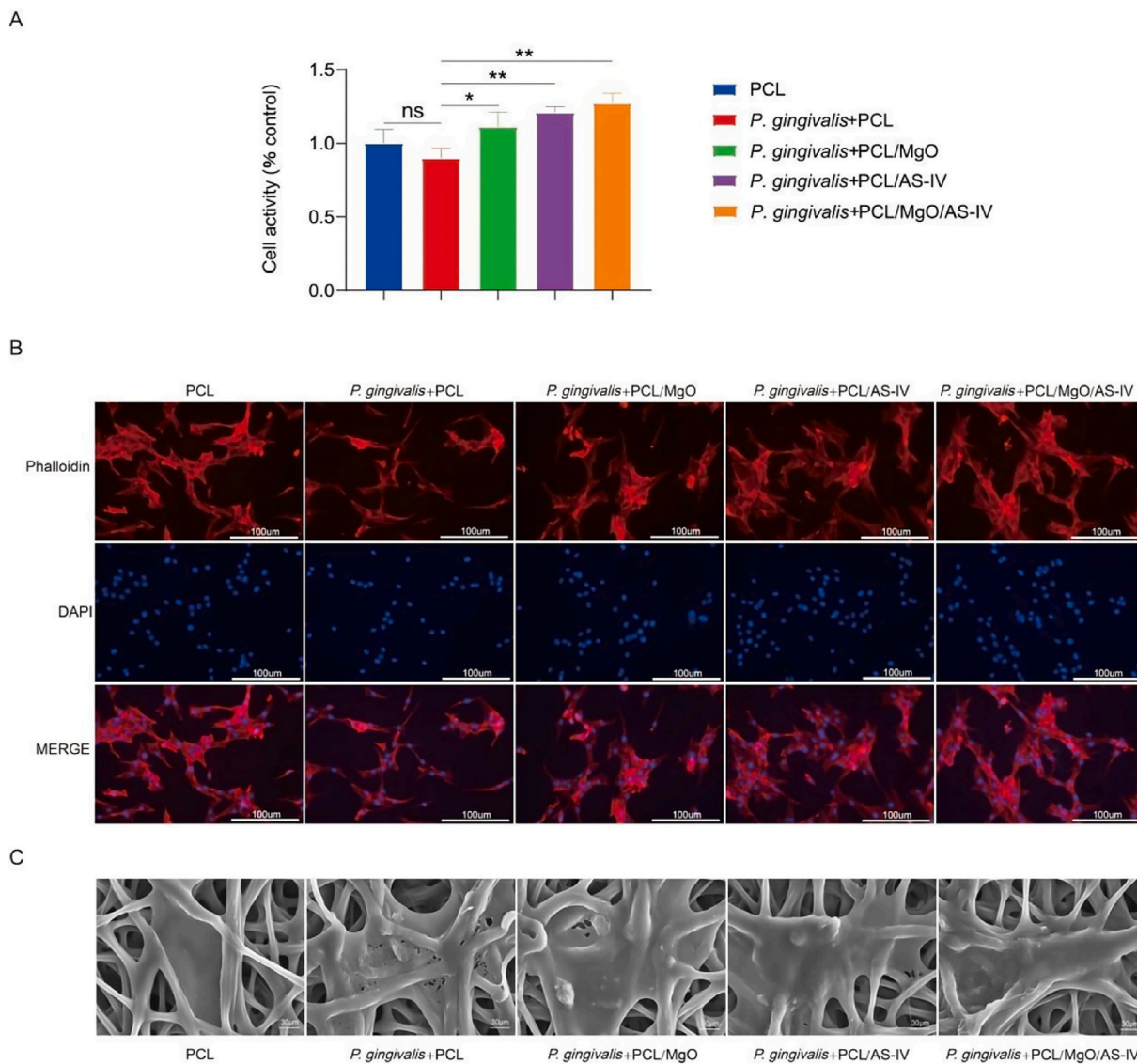
Fig. 7. Effect of PCL/MgO/AS-IV on cell proliferative activity and biocompatibility during *P.gingivalis* infection. (A) The CCK-8 assay demonstrated a significant enhancement in cell proliferation within the PCL/MgO/AS-IV group compared to the *P.gingivalis*-infected group. (B) Immunofluorescence and scanning electron microscopy (C) results revealed robust cellular growth and fully expanded cell morphology on the electrospun scaffolds across all experimental groups. (*$p < 0.05$;**$p < 0.01$;ns $p > 0.05$).

A
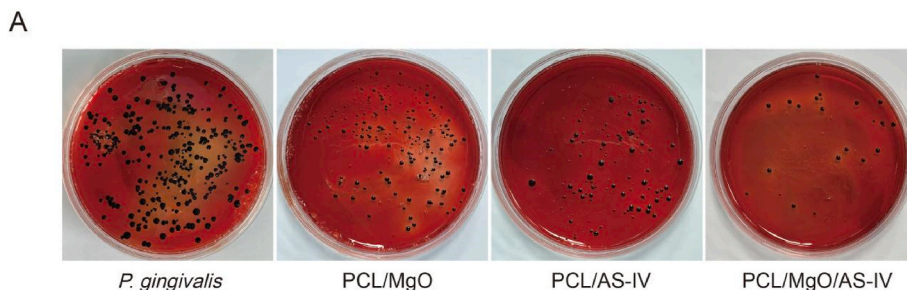
Fig. 8. The addition of PCL/MgO/AS-IV effectively inhibited the activity of *P.gingivalis*, as evidenced by a significant reduction in bacterial clusters observed in the PCL/MgO/AS-IV group compared to the control group.
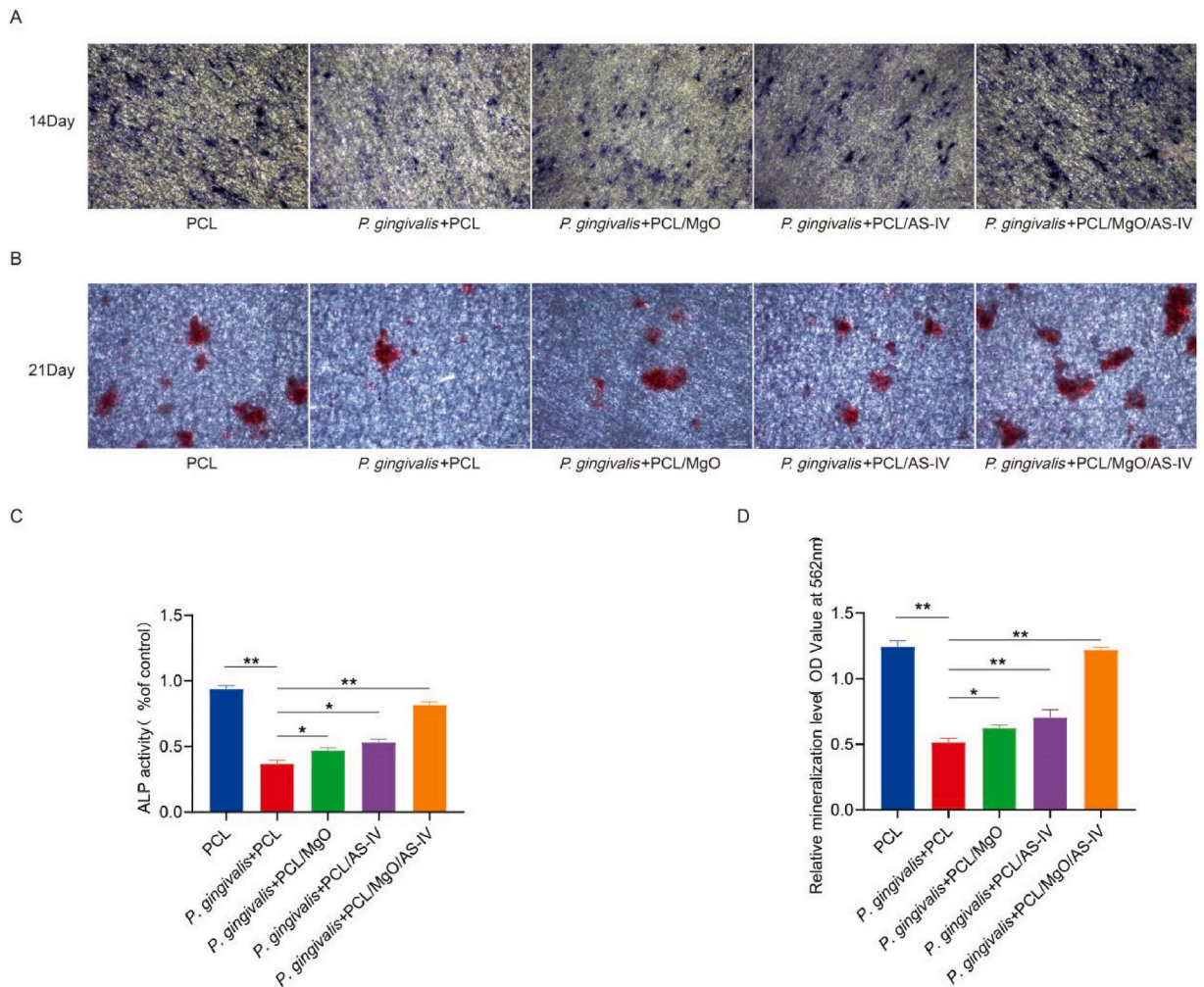
Fig. 9. Effect of PCL/MgO/AS-IV on osteogenic differentiation of MC3T3-E1 cells during *P.gingivalis* infection. After 14 days of *P.gingivalis* infection in MC3T3-E1 cells, (A) alkaline phosphatase staining revealed a significant reduction in ALP activity compared to the PCL group; however, the PCL/MgO/AS-IV group effectively enhanced cellular ALP activity expression under *P.gingivalis*-infected conditions. On day 21 after *P.gingivalis* infection in MC3T3-E1 cells, (B) Alizarin red staining demonstrated significantly lower mineral deposition in the infected group compared to the PCL group; nevertheless, the presence of PCL/MgO/AS-IV significantly promoted mineral content deposition during *P.gingivalis* infection. (*$p < 0.05$;**$p < 0.01$; ns $p > 0.05$). (For interpretation of the references to colour in this figure legend, the reader is referred to the Web version of this article.)

findings of increased BV/TV. In addition, the results of Fig. 10C showed that none of the sections of important organs in vivo showed obvious pathological changes. The above results indicate that PCL/MgO/AS-IV artificial periosteum has higher bone-contributing capacity and good biocompatibility in vivo.

3.12. PCL/MgO/AS-IV promotes the expression of osteogenic differentiation proteins through the EphB4/EphrinB2 signaling pathway

The immunoprotein blotting results depicted in Fig. 11A, B, 11C, 11D, 11E, 11F demonstrated a significant reduction in the protein expression of EphB4, ALP, OPN, and RunX2 in the *P.gingivalis*-infected group compared to the control group. Conversely, EphrinB2 protein expression appeared to be significantly up-regulated. Notably, both the PCL/MgO and PCL/AS-IV groups exhibited enhanced expression of osteogenic differentiation proteins ALP, OPN, and RunX2; however, the most pronounced increase was observed in the PCL/MgO/AS-IV group. Furthermore, when compared to the *P.gingivalis*-infected group, protein expression of EphrinB2 was significantly suppressed while that of EphB4, ALP, OPN,and RunX2 was significantly elevated in the PCL/MgO/AS-IV group. These findings suggest that regulation of osteogenic differentiation through the EphB4/EphrinB2 signaling pathway may be facilitated by PCL/MgO/AS-IV.
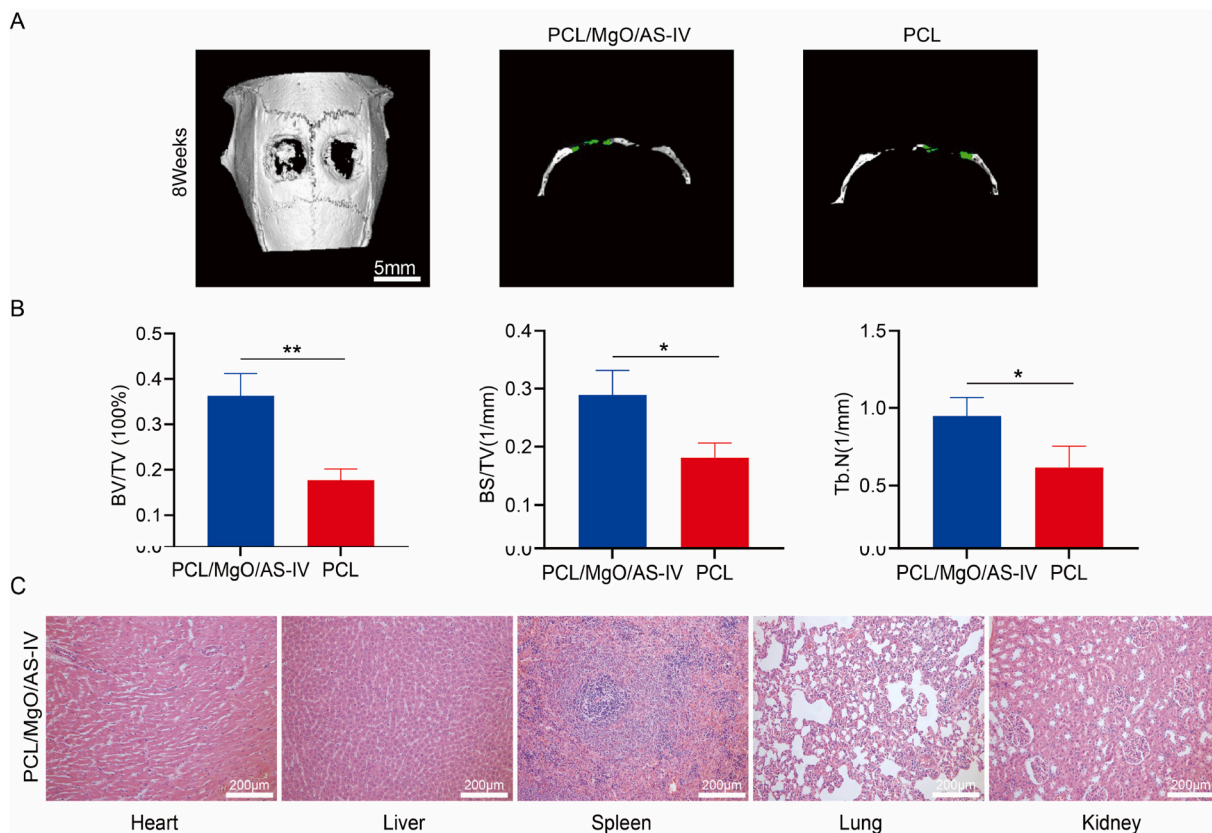
Fig. 10. Reparative effects of PCL/MgO/AS-IV artificial periosteum on bone defect regeneration. (A) Micro-CT 3D reconstructed image at week 8 of implantation. (B) Quantitative analysis of osteogenic capacity showed that the PCL/MgO/AS-IV periosteal group significantly enhanced bone defect repair compared with the PCL group. (C) The results of in vivo organ sections demonstrated that the application of PCL/MgO/AS-IV artificial periosteum did not induce significant pathological alterations in the organs. (*$p < 0.05$;**$p < 0.01$;ns $p > 0.05$).

4. Discussion

Periodontitis leads to alveolar bone loss and eventual tooth loss, presenting a significant clinical management challenge [28]. In this study, we highlight the active roles of Mg^{2+} and AS-IV in osteogenesis, two bioactive materials with promising prospects for diverse biological applications [29,30]. Furthermore, despite the widespread use of guided tissue regeneration (GTR) technology as a biological barrier to facilitate periodontal tissue regeneration in periodontal surgery, it still faces challenges such as high fabrication costs, antimicrobial resistance, and limited osteogenic capacity [31,32]. Therefore, our current work focuses on fabricating a nano-artificial periosteum incorporating MgO and AS-IV within a PCL substrate to establish a reliable platform for treating periodontal bone loss while investigating its regulatory signals during bone repair.

P.gingivalis is recognized as one of the most prominent dominant bacteria in the pathogenesis of periodontitis, capable of generating a diverse array of inflammatory factors that disrupt bone tissue repair and regeneration [33,34]. Current research on periodontal therapy for bone restoration primarily focuses on the isolated effects of materials on cells, which has certain limitations [35]. However, bone tissue loss is a consequence of prolonged inflammation, and persistent bacterial infections can better simulate the onset of periodontitis. The inflammatory response induced by living *P.gingivalis* is more intricate compared to its metabolites or ultrasound extracts and provides a closer mimicry to the pathogenesis of periodontitis as well [36]. Previous studies have demonstrated that *P. gingivalis* can persistently infect primary mouse osteoblasts for 28 days without affecting cell proliferation, using an MOI of 150 [37]. Geng et al. [36] found that continuous infection of human immortalized oral epithelial cells with *P. gingivalis* with MOI = 1 for up to 23 weeks promotes cell proliferation, migration, and invasive capacity. Ha et al. [37] demonstrated that continuous infection of cellular oral squamous cell carcinoma (OSCC) with *P. gingivalis* with MOI = 100 for 5 weeks enhanced cell migration and invasion, and we hypothesized that the difference in MOI selection might be related to different organelles selected. In this experiment, MC3T3-E1 cells were initially infected with *P.gingivalis* at an MOI of 50; live-dead cell staining and CCK-8 assay results revealed a slight decrease in cell density compared to the control group under long-term infection conditions but did not reach statistical significance. These findings suggest that persistent infection of *P. gingivalis* does not exert an impact on the proliferation of MC3T3-E1 cells and effectively recapitulates the pathogenesis of periodontitis.

Magnesium actively participates in inducing osteogenic differentiation both in vivo and in vitro, while AS-IV demonstrates an
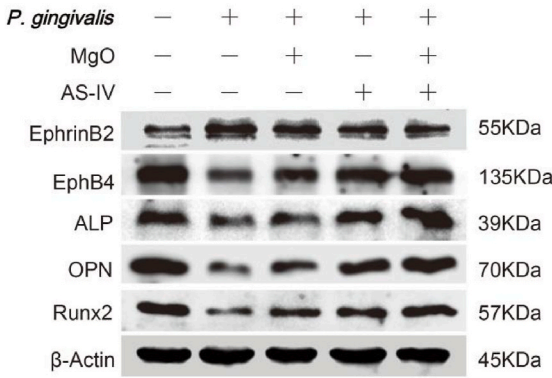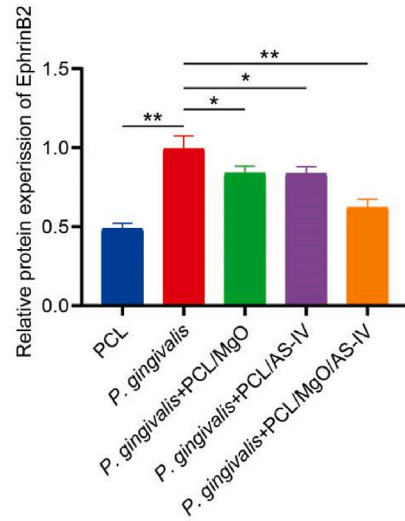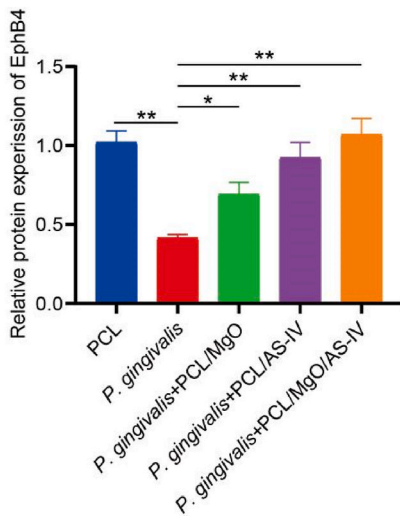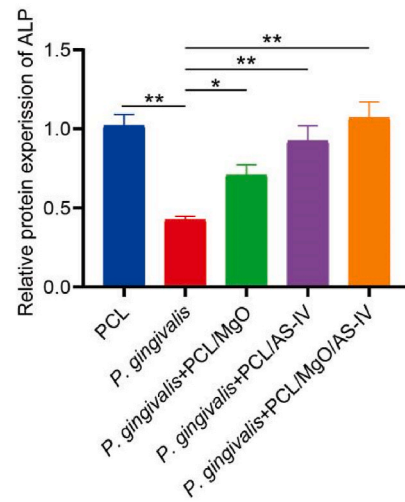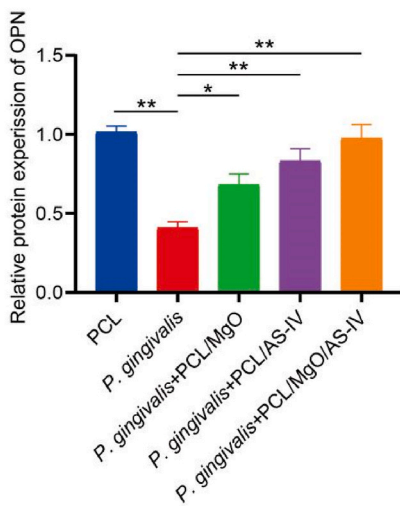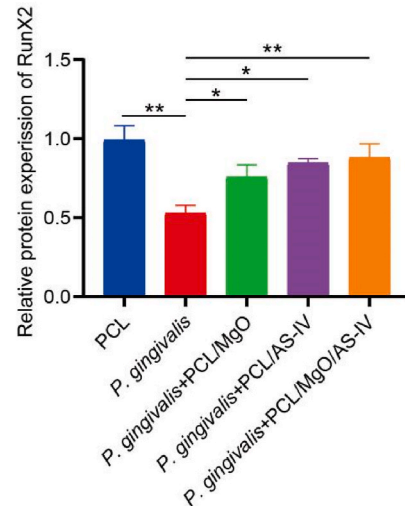
Fig. 11. Effect of PCL/MgO/AS-IV on osteogenic differentiation proteins during *P.gingivalis* infection. To gain further insights into the mechanism underlying the contribution of PCL/MgO/AS-IV to osteogenic differentiation under *P.gingivalis* infection, (A) Immunoprotein blotting and (B–F) quantification revealed a significant increase in EphrinB2 expression in the *P.gingivalis*-infected group compared to the control group, accompanied by a significant reduction in EphB4 and osteogenic differentiation-associated protein expression levels. In contrast, compared to the *P.gingivalis*-infected group, the PCL/MgO/AS-IV group exhibited a significant decrease in EphrinB2 protein expression but a substantial enhancement in EphB4 and osteogenic differentiation-related protein expressions. (*$p < 0.05$;**$p < 0.01$;ns $p > 0.05$).*

equally effective enhancement of osteogenic differentiation. Consequently, AS-IV and Mg^{2+} have been investigated as biologically active substitutes for bone reconstruction [38,39]. Therefore, we examined the proliferative viability of MC3T3-E1 cells under *P. gingivalis* infection using Mg^{2+} and AS-IV. Interestingly, the *P.gingivalis*-infected group exhibited a slight increase in cell density at 24 h compared to the control group—a potential defensive proliferation response to *P.gingivalis* stimulation by the cells. Moreover, the combined effect of Mg^{2+} and AS-IV significantly promoted time-dependent cell proliferation compared to the *P.gingivalis*-infected group. Meanwhile, the cell morphology results revealed that in the *P.gingivalis* infected group, certain cells exhibited a wrinkled morphology with limited stretching; however, when treated with a combination of Mg^{2+} and AS-IV, the cells displayed complete morphological characteristics, thereby significantly enhancing their growth status under *P.gingivalis* infection. These findings suggest excellent biocompatibility between the two bioactives and MC3T3-E1 cells.

ROS serves as a crucial biomarker that responds to intracellular inflammation levels. In the presence of inflammatory stimuli and cellular passaging, senescent cells exhibit a rapid increase in intracellular ROS levels and subsequent oxidative damage [40]. Our findings demonstrate that persistent *P.gingivalis* infection significantly upregulates intracellular ROS expression; however, both Mg^{2+} and AS-IV effectively inhibit this expression. Moreover, the combined effect of Mg^{2+} and AS-IV leads to an even more pronounced suppression of intracellular ROS expression. This suggests that their combination can mitigate irreversible cell damage caused by DNA breaks and protein degradation [41]. Consequently, our results provide reliable evidence supporting the ability of Mg^{2+} and AS-IV to effectively impede inflammation progression while minimizing peripheral cell destruction induced by inflammation, thereby highlighting their excellent biocompatibility.

Enhancing osteogenic activity is a crucial factor in the bone repair process [42]. In our study, alkaline phosphatase staining and alizarin red staining revealed that the combined effect of Mg^{2+} and AS-IV significantly augmented the expression of osteogenic activity during *P.gingivalis* infection, indicating a robust synergistic interaction between these two factors. Moreover, previous studies have demonstrated that Mg^{2+} and AS-IV exhibit a synergistic effect in promoting cell proliferation, attenuating intracellular ROS expression under *P.gingivalis* infection, and facilitating osteogenic differentiation. However, it should be noted that magnesium powder can induce side effects when dissolved in the culture medium by elevating solution pH and creating an alkaline environment that inhibits cell growth [43]. Additionally, the drug's direct action on cells induces both synaptic and toxic effects [44]. As a promising carrier for nanomaterials in the future, PCL exhibits excellent biocompatibility and enables encapsulation of bioactive agents within the nuclear layer to facilitate sustained drug transport [45]. Therefore, we developed a multifunctional nanoplatform using PCL as a basis to fabricate PCL/MgO/AS-IV artificial periosteum for evaluating its antimicrobial and osteogenic properties. Scanning electron microscopy analysis revealed negligible changes in diameter upon addition of MgO and AS-IV. Conversely, XRD results confirmed characteristic peaks corresponding to MgO presence in both the PCL/MgO group and the PCL/MgO/AS-IV group. However, no alterations were observed in characteristic peaks between the PCL/AS-IV group and the control PCL group, possibly due to minimal AS-IV addition and its dispersion within the electrospinning solution not significantly affecting overall crystallization degree of PCL. The presence of AS-IV characteristic peaks in the PCL/AS-IV group and PCL/MgO/AS-IV group was confirmed by FTIR spectroscopy, indicating successful incorporation of AS-IV. Interestingly, a C═C stretching vibrational peak at 1580 cm^{-1} emerged in the PCL/MgO/AS-IV group, suggesting the formation of a C═C bond between PCL and AS-IV facilitated by MgO addition. These findings demonstrate successful integration of bioactive component MgO with AS-IV into the artificial periosteum. WCA experiments revealed that compared to the PCL group, the water contact angle decreased in the PCL/MgO/AS-IV group, implying enhanced hydrophilicity resulting from combined application of MgO and AS-IV. Furthermore, the PCL/MgO/AS-IV artificial periosteum exhibited significant enhancement in MC3T3-E1 cell proliferation under bacterial infection, as confirmed by both CCK-8 proliferation assay and cytomorphologic results. Scanning electron microscopy and fluorescence analysis demonstrated excellent cellular adhesion and stretching capabilities of the cells on the periosteal surface, thus providing compelling evidence for the favorable biocompatibility of the PCL/MgO/AS-IV artificial periosteum. Moreover, unlike pure PCL which takes approximately 2–3 years to degrade completely in vivo [46], degradation of this artificial periosteum can facilitate complex bone repair processes. Additionally, release of antibacterial and osteogenic active ingredients from the descending interpretation of the artificial periosteum can expedite osteogenesis and promote periodontitis healing. In our study, the PCL/AS-IV group and the PCL/MgO/AS-IV group exhibited rapid release of AS-IV during the initial stage, leading to an increased local drug concentration in the inflammatory environment and optimal utilization of its anti-inflammatory effects. Consequently, effective alleviation of local inflammation facilitated more favorable conditions for subsequent osteogenesis. Furthermore, as the artificial periosteum gradually degraded, a sustained release of AS-IV occurred alongside Mg^{2+}, acting synergistically as dual active substances to promote osseointegration.

The Mg^{2+} release in the PCL/MgO/AS-IV group was comparable to that of the PCL/MgO group, but with a faster rate due to AS-IV's ability to enhance hydrophilicity and accelerate degradation of the artificial periosteum, leading to quicker Mg^{2+} release. It is evident that slow Mg^{2+} release aids in stabilizing pH levels within the environment, creating favorable conditions for cell adhesion and growth. Furthermore, prolonged existence of Mg^{2+}, along with AS-IV, within the degrading artificial periosteum provides optimal conditions for long-term and complex bone repair processes ultimately resulting in ideal therapeutic outcomes.

The excellent antimicrobial properties play a crucial role in evaluating the efficacy of artificial bone membrane preparation. In the antimicrobial experiments, we observed that both PCL/MgO and PCL/AS-IV exhibited inhibitory effects on the growth of *P.gingivalis*, but the combination of MgO and AS-IV in PCL/MgO/AS-IV demonstrated superior antimicrobial performance. This suggests that their synergistic action can further enhance their respective biological properties, effectively resisting periodontal tissue destruction caused by *P.gingivalis*. Moreover, nanomaterials have been shown to influence cell renewal and osteogenic differentiation [47,48]. Encouragingly, under infected conditions with *P.gingivalis*, the artificial periosteum composed of PCL/MgO/AS-IV significantly enhanced ALP activity expression and promoted late-stage osteogenic mineralized nodule formation. Meanwhile, in vivo experiments provided additional validation for the favorable impact of PCL/MgO/AS-IV artificial periosteum on osteoblast behavior, demonstrating significant enhancement of bone regeneration. This can be attributed to the ability of the electrostatically spun artificial periosteum structure to closely mimic the extracellular matrix. The Micro-CT quantification results revealed that the osteogenesis observed in the PCL/MgO/AS-IV artificial periosteum group was approximately twofold higher compared to the PCL group, thereby further confirming the osteogenic potential of MgO and AS-IV. Combining the results of in vitro degradation experiments and cellular experiments, it can be concluded that Mg^{2+} and AS-IV released by degradation of PCL/MgO/AS-IV artificial periosteum have a synergistic bone-enhancing effect. Furthermore, histological analysis of various organs in the PCL/MgO/AS-IV artificial periosteum group demonstrated excellent biocompatibility. Therefore, PCL/MgO/AS-IV artificial periosteum holds significant promise as a suitable material for guided bone regeneration (GBR) or guided tissue regeneration (GTR) in periodontitis treatment.

The study confirms the essential involvement of the EphB4/EphrinB2 bidirectional signaling pathway in the process of bone reconstruction [49]. Activation of the EphB4 receptor induces positive signaling to enhance osteoblast differentiation, while activation of the EphrinB2 ligand triggers negative signaling to inhibit osteoclast differentiation and promote apoptosis [50,51]. Therefore, in this study, we further investigated the role of PCL/MgO/AS-IV in modulating these relevant signaling pathways during osteogenic differentiation. Immunoprotein blotting results revealed a significant downregulation of ALP, OPN, RunX2, and EphB4 expression in the *P.gingivalis*-infected group compared to the control group, accompanied by a substantial upregulation of EphrinB2 expression. In contrast, compared to the *P.gingivalis*-infected group, treatment with PCL/MgO/AS-IV exhibited remarkable upregulation of protein expression levels for EphB4 and key osteogenic markers including ALP, OPN, and RunX2; concurrently downregulating EphrinB2 expression. These findings suggest that PCL/MgO/AS-IV artificial periosteum promotes osteogenic repair through activation of bidirectional EphB4/EphrinB2 signaling pathway. However, further investigations are warranted to elucidate specific roles played by MgO and AS-IV in regulating this bidirectional signaling.

5. Conclusion

In this study, we utilized *P. gingivalis* to establish a persistent infection in MC3T3-E1 cells and demonstrated that the combined administration of Mg^{2+} and AS-IV effectively suppressed the inflammatory response while promoting cell proliferation and osteogenic differentiation during *P. gingivalis* infection. At the same time, we prepared a PCL artificial periosteum incorporating MgO and AS-IV. In vitro experimental results demonstrated excellent biocompatibility between PCL/MgO/AS-IV artificial periosteum and MC3T3-E1 cells, exhibiting remarkable antimicrobial effects while effectively promoting osteogenic differentiation of MC3T3-E1 cells under P. gingivalis infection. The in vivo experiments confirmed the exceptional bone-enhancing capacity of the PCL/MgO/AS-IV artificial periosteum, effectively facilitating bone defect repair. Moreover, our findings revealed that the PCL/MgO/AS-IV artificial periosteum facilitated bone defect repair by activating EphB4/EphrinB2 bidirectional signaling pathway. Collectively, these results highlight the multifunctional properties of the PCL/MgO/AS-IV artificial periosteum and its promising potential for future applications in bone defect repair for periodontitis treatment.

Data availability statement

No data was used for the research described in the article.

CRediT authorship contribution statement

Wei Wang: Writing – original draft, Validation, Software, Methodology, Investigation, Formal analysis, Data curation, Conceptualization. **Dan-Fang Sun:** Visualization, Validation, Data curation. **Hui-Xia Cui:** Writing – review & editing, Resources, Methodology, Investigation, Conceptualization. **Wen-Lu Zhang:** Writing – review & editing, Supervision, Resources, Project administration, Methodology, Funding acquisition.

Declaration of competing interest

The authors declare the following financial interests/personal relationships which may be considered as potential competing interestsWen-lu Zhang reports financial support was provided byBeijing Xisike Clinical Oncology Research Foundation, No. 662202304027. If there are other authors, they declare that they have no known competing financial interests or personal relationships that could have appeared to influence the work reported in this paper.

Appendix A. Supplementary data

Supplementary data to this article can be found online at https://doi.org/10.1016/j.heliyon.2024.e32036.

References

[1] R. Chen, et al., Anti-Porphyromonas gingivalis nanotherapy for maintaining bacterial homeostasis in periodontitis, Int J Antimicrob Agents 61 (6) (2023) 106801.
[2] N. Yan, et al., Penetrating macrophage-based nanoformulation for periodontitis treatment, ACS Nano 16 (11) (2022) 18253–18265.
[3] M. Sanz, et al., Periodontitis and cardiovascular diseases: consensus report, J Clin Periodontol 47 (3) (2020) 268–288.
[4] T. Kwon, I.B. Lamster, L. Levin, Current concepts in the management of periodontitis, Int Dent J 71 (6) (2021) 462–476.
[5] W. Peng, et al., MgO nanoparticles-incorporated PCL/Gelatin-Derived coaxial electrospinning nanocellulose membranes for periodontal tissue regeneration, Front Bioeng Biotechnol 9 (2021) 668428.
[6] L. Chen, et al., Collagen membrane derived from fish scales for application in bone tissue engineering, Polymers (Basel) 14 (13) (2022).
[7] F.M. Chen, Periodontal tissue engineering and regeneration], Zhonghua Kou Qiang Yi Xue Za Zhi 52 (10) (2017) 610–614.
[8] J. Miszuk, et al., An elastic mineralized 3D electrospun PCL nanofibrous scaffold for drug release and bone tissue engineering, ACS Appl Bio Mater 4 (4) (2021) 3639–3648.
[9] C. Meng, et al., Heterogeneous porous PLLA/PCL fibrous scaffold for bone tissue regeneration, Int J Biol Macromol 235 (2023) 123781.
[10] Y. Wang, et al., Biomimetic glycopeptide hydrogel coated PCL/nHA scaffold for enhanced cranial bone regeneration via macrophage M2 polarization-induced osteo-immunomodulation, Biomaterials 285 (2022) 121538.
[11] H.A. Owida, et al., Recent applications of electrospun nanofibrous scaffold in tissue engineering, Appl Bionics Biomech 2022 (2022) 1953861.
[12] Y. He, et al., Study on the mechanism of antibacterial action of magnesium oxide nanoparticles against foodborne pathogens, J Nanobiotechnology 14 (1) (2016) 54.
[13] S. Ni, X.B. Xiong, X.Y. Ni, MgCl2 promotes mouse mesenchymal stem cell osteogenic differentiation by activating the p38/Osx/Runx2 signaling pathway, Mol Med Rep 22 (5) (2020) 3904–3910.
[14] C. Ferreira, et al., Advanced face mask filters based on PCL electrospun meshes dopped with antimicrobial MgO and CuO nanoparticles, Polymers (Basel) 14 (16) (2022).
[15] W. Peng, et al., MgO nanoparticles-incorporated PCL/Gelatin-Derived coaxial electrospinning nanocellulose membranes for periodontal tissue regeneration, Front Bioeng Biotechnol 9 (2021) 668428.
[16] D. Zhang, et al., Collaborative design of MgO/FeO(x) nanosheets on titanium: combining therapy with regeneration, Small 19 (5) (2023) e2204852.
[17] Y. Zang, et al., An updated role of astragaloside IV in heart failure, Biomed Pharmacother 126 (2020) 110012.
[18] Y. Liang, et al., Pharmacological effects of astragaloside IV: a review, Molecules 28 (16) (2023).
[19] C. Wu, et al., Astragaloside reduces toxic effect of periodontal ligament fibroblasts induced by lipopolysaccharide, Arch Biochem Biophys 744 (2023) 109693.
[20] J. Delgado-Calle, T. Bellido, The osteocyte as a signaling cell, Physiol Rev 102 (1) (2022) 379–410.
[21] M. Li, et al., Lipopolysaccharides affect compressed periodontal ligament cells via Eph-ephrin signaling, Oral Dis 28 (6) (2022) 1662–1673.
[22] Y. Chen, et al., Single-cell RNA landscape of the osteoimmunology microenvironment in periodontitis, Theranostics 12 (3) (2022) 1074–1096.
[23] M. Li, et al., Inhibition of RANKL-induced osteoclastogenesis through the suppression of the ERK signaling pathway by astragaloside IV and attenuation of titanium-particle-induced osteolysis, Int J Mol Med 36 (5) (2015) 1335–1344.
[24] W.B. Jing, et al., Astragaloside positively regulated osteogenic differentiation of pre-osteoblast MC3T3-E1 through PI3K/Akt signaling pathway, J Orthop Surg Res 16 (1) (2021) 579.
[25] Y. Cao, Q. Lv, Y. Li, Astragaloside IV improves tibial defect in rats and promotes proliferation and osteogenic differentiation of hBMSCs through MiR-124-3p.1/ STAT3 Axis, J Nat Prod 84 (2) (2021) 287–297.
[26] Z. Yuan, et al., Dual-controlled release of icariin/Mg(2+) from biodegradable microspheres and their synergistic upregulation effect on bone regeneration, Adv Healthc Mater 9 (11) (2020) e2000211.
[27] A. Bhattacharjee, Y. Jo, S. Bose, In vivo and in vitro properties evaluation of curcumin loaded MgO doped 3D printed TCP scaffolds, J Mater Chem B 11 (21) (2023) 4725–4739.
[28] B. Yu, C.Y. Wang, Osteoporosis and periodontal diseases - an update on their association and mechanistic links, Periodontol 89 (1) (2000) 99–113, 2022.
[29] X. Wei, et al., Magnesium surface-activated 3D printed porous PEEK scaffolds for in vivo osseointegration by promoting angiogenesis and osteogenesis, Bioact Mater 20 (2023) 16–28.
[30] F. Wang, et al., Accelerated bone regeneration by astragaloside IV through stimulating the coupling of osteogenesis and angiogenesis, Int J Biol Sci 17 (7) (2021) 1821–1836.
[31] P. Ming, et al., Biomimetic design and fabrication of sericin-hydroxyapatite based membranes with osteogenic activity for periodontal tissue regeneration, Front Bioeng Biotechnol 10 (2022) 899293.
[32] A.M. Tryba, et al., Surface functionalization of poly(l-lactide-co-glycolide) membranes with RGD-grafted poly(2-oxazoline) for periodontal tissue engineering, J Funct Biomater 13 (1) (2022).
[33] L. Wang, et al., SAP deficiency aggravates periodontitis possibly via C5a-C5aR signaling-mediated defective macrophage phagocytosis of Porphyromonas gingivalis, J Adv Res 50 (2023) 55–68.
[34] Q. Tan, et al., Periodontitis pathogen Porphyromonas gingivalis promotes pancreatic tumorigenesis via neutrophil elastase from tumor-associated neutrophils, Gut Microbes 14 (1) (2022) 2073785.
[35] F.C. Chen, et al., Effect of nano zinc oxide on proliferation and toxicity of human gingival cells, Hum Exp Toxicol 41 (2022) 9603271221080236.
[36] T. Ohno, et al., Proinflammatory gene expression in mouse ST2 cell line in response to infection by Porphyromonas gingivalis, Microbes Infect 8 (4) (2006) 1025–1034.
[37] W. Zhang, et al., Porphyromonas gingivalis invades osteoblasts and inhibits bone formation, Microbes Infect 12 (11) (2010) 838–845.
[38] A.M. Dias, et al., Magnesium (Mg2 +), strontium (Sr2 +), and zinc (Zn2 +) Co-substituted bone cements based on nano-hydroxyapatite/monetite for bone regeneration, Biol Trace Elem Res 201 (6) (2023) 2963–2981.
[39] X. Lian, et al., Cytological mechanism of astragaloside IV in promoting repair of bone defects, J Biol Regul Homeost Agents 33 (2) (2019) 511–516.
[40] L. Ma, et al., Maintained properties of aged dental pulp stem cells for superior periodontal tissue regeneration, Aging Dis 10 (4) (2019) 793–806.
[41] C. Mahapatra, et al., Nano-shape varied cerium oxide nanomaterials rescue human dental stem cells from oxidative insult through intracellular or extracellular actions, Acta Biomater 50 (2017) 142–153.
[42] L. Hu, et al., MiR-1224-5p modulates osteogenesis by coordinating osteoblast/osteoclast differentiation via the Rap1 signaling target ADCY2, Exp Mol Med 54 (7) (2022) 961–972.
[43] J. Walker, et al., Magnesium biomaterials for orthopedic application: a review from a biological perspective, J Biomed Mater Res B Appl Biomater 102 (6) (2014) 1316–1331.
[44] Y. Huang, et al., Icariin-loaded electrospun PCL/gelatin sub-microfiber mat for preventing epidural adhesions after laminectomy, Int J Nanomedicine 13 (2018) 4831–4844.

[45] A. Khalf, S.V. Madihally, Recent advances in multiaxial electrospinning for drug delivery, Eur J Pharm Biopharm 112 (2017) 1–17.

[46] J.R. Dias, et al., Electrospun polycaprolactone (PCL) degradation: an in vitro and in vivo study, Polymers (Basel) 14 (16) (2022).

[47] J.J. Li, N. Kawazoe, G. Chen, Gold nanoparticles with different charge and moiety induce differential cell response on mesenchymal stem cell osteogenesis, Biomaterials 54 (2015) 226–236.

[48] J. Qiu, et al., Effects of graphene quantum dots on the self-renewal and differentiation of mesenchymal stem cells, Adv Healthc Mater 5 (6) (2016) 702–710.

[49] A. Arthur, S. Gronthos, Eph-Ephrin signaling mediates cross-talk within the bone microenvironment, Front Cell Dev Biol 9 (2021) 598612.

[50] Y. Zhang, et al., ED-71 inhibited osteoclastogenesis by enhancing EphrinB2-EphB4 signaling between osteoclasts and osteoblasts in osteoporosis, Cell Signal 96 (2022) 110376.

[51] M. Frye, et al., EphrinB2-EphB4 signalling provides Rho-mediated homeostatic control of lymphatic endothelial cell junction integrity, Elife 9 (2020).